Model for Stress-Dependent Hysteresis in Electrical Steel Sheets Including Orthotropic Anisotropy

P. Rasilo[1,2], S. Steentjes[3], A. Belahcen[2], R. Kouhia[4], and K. Hameyer[3]

[1]Laboratory of Electrical Energy Engineering, Tampere University of Technology, 33720 Tampere, Finland
[2]Department of Electrical Engineering and Automation, Aalto University, 02150 Espoo, Finland
[3]Institute of Electrical Machines (IEM), RWTH Aachen University, 52062 Aachen, Germany
[4]Laboratory of Civil Engineering, Tampere University of Technology, 33720 Tampere, Finland

An energy-based approach for anisotropic modeling of stress-dependent magnetization curves in electrical steel sheets is presented. The model is based on an orthotropic extension of an existing isotropic thermodynamic model and coupling to the Jiles–Atherton model of hysteresis. The model fits well to experimental results under uniaxial excitation, and it is numerically tested under rotational fields.

Index Terms— **Anisotropy, hysteresis, Jiles–Atherton (JA) model, magnetic materials, magnetostriction, stress.**

I. Introduction

MAGNETIC behavior of electrical steel sheets under mechanical stress is a rather complicated problem due to its intrinsic three-dimensionality, but its accurate and effective representation is indispensable for the design of electromechanic energy transducers, such as rotating electrical machines. Mechanical stress is inherent in processed parts from processing and manufacturing as well as induced by the operation of the machine, e.g., centrifugal force or magnetic forces. This interacts with the material heterogeneity and the crystallographic orientation of the individual grains. As a result of this multiscale interaction the stress-dependent magnetization behavior is heavily dependent on the direction of the magnetic field with respect to the grain orientations [1].

The magnetomechanical coupling is the result of intricate mechanisms at different spatial scales [2] and can be modeled using micromagnetic or multiscale approaches [2]. Inherent to these approaches are prohibitive computation times, making these unsuitable for an implementation into numerical tools. For this reason, simplified models were developed that either treat the multiaxial problem in uniaxial models starting from the definition of an equivalent stress [3] or simplify the multiscale problem through the neglection of hysteresis or treatment of the polycrystal as a fictitious single crystal [4], [5]. Thermodynamic approaches base on a magnetomechanical definition of a free energy density, and were recently extended to the hysteretic case [6]. These emerging approaches allow accurately accounting for arbitrary orientations between the magnetic field and the stress, but so far only isotropic or anhysteretic models have been presented.

In this paper, the thermodynamic approach by means of a field- and stress-dependent free energy density is extended for modeling stress-dependent magnetization curves considering hysteresis and orthotropic anisotropy. Comparisons to measured quasi-static magnetization curves and hysteresis loops are discussed.

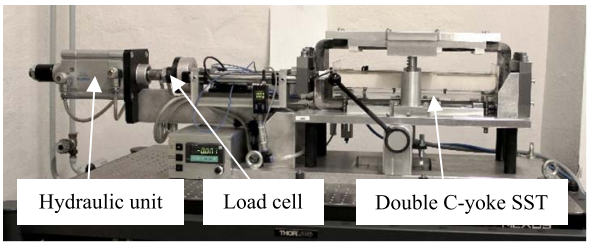

Fig. 1. SST with hydraulic loading unit (IEM RWTH).

II. Methods

A. Measurements

Experiments were performed on a uniaxial single sheet tester (SST) at the Institute of Electrical Machines. The samples are 600 mm × 100 mm in size, cut by water jet from two different 0.5-mm fully processed nonoriented 2.4 % Si–Fe grades. The two materials have similar alloy content, but different magnetic texture and grain size. They are termed as Material 1 and Material 2. The samples were not annealed in order to better meet the conditions of the final application, such as an electrical machine. The setup is equipped with a tensile and compression hydraulic loading unit and enables the application of uniaxial mechanical stress collinear to the magnetic flux up to a maximum force of 5 kN, see Fig. 1.

The SST is incorporated into a computer-aided setup according to the international standard IEC 60404–3 and the magnetic flux is controlled to be sinusoidal in time with a form factor deviation of less than 1% from $\pi/\sqrt{8}$. In order to minimize the effect of induced eddy currents, that is having a uniformly distributed B, the magnetizing frequency is restricted to 3 Hz. For given values of mechanical stress σ and controlled B the magnetic field H was measured, which allows

Manuscript received November 15, 2016; revised December 20, 2016 and January 13, 2017; accepted January 24, 2017. Date of publication January 26, 2017; date of current version May 26, 2017. Corresponding author: P. Rasilo (e-mail: paavo.rasilo@tut.fi).

Color versions of one or more of the figures in this paper are available online at http://ieeexplore.ieee.org.

Digital Object Identifier 10.1109/TMAG.2017.2659784

constructing a uniform grid (H, σ). Experiments are performed in different angles relative to the rolling direction, i.e., 0° [rolling direction (RD)] and 90° [transversal direction (TD)].

B. Anhysteretic Isotropic Constitutive Law

An isotropic magnetoelastic model is derived first. We are looking for a thermodynamic free energy density ϕ_{me} as a function of the magnetic field strength vector $\boldsymbol{H}$ and stress tensor $\boldsymbol{\sigma}$, from which we can derive the magnetization vector $\boldsymbol{M}$ and magnetostriction tensor $\boldsymbol{\lambda}$ as

$$\boldsymbol{M}(\boldsymbol{H},\boldsymbol{\sigma}) = \left(\frac{\partial \phi_{\mathrm{me}}(\boldsymbol{H},\boldsymbol{\sigma})}{\partial \boldsymbol{H}}\right)^{\mathrm{T}} \tag{1}$$

$$\boldsymbol{\lambda}(\boldsymbol{H},\boldsymbol{\sigma}) = \frac{\partial \phi_{\mathrm{me}}(\boldsymbol{H},\boldsymbol{\sigma})}{\partial \boldsymbol{\sigma}}. \tag{2}$$

In an isotropic case the energy density can only depend on invariants (see [6] and references therein)

$$\begin{aligned} I_1 = \operatorname{tr}\boldsymbol{\sigma}, \quad I_2 = \operatorname{tr}(\boldsymbol{\sigma}^2), \quad I_3 = \det\boldsymbol{\sigma} \\ I_4 = \boldsymbol{H}\cdot\boldsymbol{H}, \quad I_5 = \boldsymbol{H}\cdot(\boldsymbol{s}\boldsymbol{H}), \quad I_6 = \boldsymbol{H}\cdot(\boldsymbol{s}^2\boldsymbol{H}) \end{aligned} \tag{3}$$

where $\boldsymbol{s} = \boldsymbol{\sigma} - 1/3(\operatorname{tr}\boldsymbol{\sigma})\boldsymbol{I}$ is the deviatoric part of the stress ($\boldsymbol{I}$ being the unit tensor). Invariants I_1–I_3 do not affect the field strength and are thus not considered here. In addition, when we only have uniaxial measurement data for

$$\boldsymbol{H} = \begin{bmatrix} H \\ 0 \\ 0 \end{bmatrix} \quad \text{and } \boldsymbol{\sigma} = \begin{bmatrix} \sigma & 0 & 0 \\ 0 & 0 & 0 \\ 0 & 0 & 0 \end{bmatrix} \tag{4}$$

invariants I_4–I_6 become

$$I_4 = H^2, \quad I_5 = \frac{2}{3}H^2\sigma \quad \text{and } I_6 = \frac{4}{9}H^2\sigma^2 \tag{5}$$

making one of the invariants dependent on the other two. Thus, when identifying the model from unidirectional data, we can eliminate one of the invariants. In this case, we eliminate I_6. All three invariants can be considered if measured data are available for magnetization curves under other stress states, which affect I_6, e.g., shear stress.

The problem has now been reduced to finding $\phi_{\mathrm{me}}(I_4, I_5)$. Analytical derivation of a suitable expression for this function from physical principles is extremely challenging. We thus aim to replace the function by direct interpolation from the measurement data. However, with uniformly distributed H and σ, invariants I_4 and I_5 are nonuniformly distributed, which complicates the interpolation. It is therefore simpler to express the energy as $\phi_{\mathrm{me}}(u, v)$ using two auxiliary variables

$$u = \sqrt{I_4} \quad \text{and } v = \frac{I_5}{I_4} \tag{6}$$

which, in the unidirectional case, reduce to

$$u = |H| \quad \text{and } v = \frac{2}{3}\sigma \tag{7}$$

which are uniform. Equation (6) can also be straightforwardly applied in the case of multiaxial fields (the case $I_4 = 0$ is trivial and leads to $\boldsymbol{M} = \boldsymbol{0}$). Equation (1) now becomes

$$\boldsymbol{M} = \phi_{\mathrm{me},u}\left(\frac{\partial u}{\partial \boldsymbol{H}}\right)^{\mathrm{T}} + \phi_{\mathrm{me},v}\left(\frac{\partial v}{\partial \boldsymbol{H}}\right)^{\mathrm{T}} \tag{8}$$

where $\phi_{\mathrm{me},u}$ and $\phi_{\mathrm{me},v}$ mean the partial derivatives of $\phi_{\mathrm{me}}(u, v)$. In the unidirectional case $\partial v/\partial \boldsymbol{H} = \partial\sigma/\partial\boldsymbol{H} = \boldsymbol{0}$, and $\phi_{\mathrm{me},u}$ equals the measured unidirectional magnetization M. Without measurements of the magnetostriction, we cannot directly obtain $\phi_{\mathrm{me},v}$ from the unidirectional measurements. However, since the magnetoelastic free energy density ϕ_{me} should not yield any magnetostriction in the absence of $\boldsymbol{H}$, it cannot contain any terms depending only on σ or v. We can thus obtain $\phi_{\mathrm{me},v}$ as

$$\phi_{\mathrm{me},v}(u, v) = \frac{\partial}{\partial v}\int \phi_{\mathrm{me},u}(u, v)du. \tag{9}$$

This integration is done by approximating the measured $\phi_{\mathrm{me},u}(u, v)$ with a bipolynomial B-spline which has a quadratic dependence on u and cubic dependence on v, and then integrating and differentiating the spline analytically. The integration yields the energy ϕ_{me} as a bicubic spline expression of u and v lying in the rectangle (m, n) of the uniform grid: $(u, v) \in [u_{m-1}, u_m] \times [v_{n-1}, v_n]$. The magnetization (8) in rectangle (m, n) is obtained by differentiating the spline with respect to $\boldsymbol{H}$

$$\boldsymbol{M}_{mn} = \sum_{i=0}^{3}\sum_{j=0}^{3} p_{mn,ij}\left[iu^{i-1}v^j\left(\frac{\partial u}{\partial \boldsymbol{H}}\right)^{\mathrm{T}} + ju^i v^{j-1}\left(\frac{\partial v}{\partial \boldsymbol{H}}\right)^{\mathrm{T}}\right] \tag{10}$$

where $p_{mn,ij}$ are the spline coefficients in this rectangle.

C. Hysteresis

The hysteretic magnetization behavior is modeled with the vector Jiles–Atherton (JA) model. The stress-independent model has been comprehensively described in [7]. The model can be summarized with the following five equations:

$$\boldsymbol{H}_{\mathrm{eff}} = \boldsymbol{H} + \alpha\boldsymbol{M} \tag{11}$$

$$\boldsymbol{M}_{\mathrm{an}} = \left(\frac{\partial \phi_{\mathrm{me}}(\boldsymbol{H}_{\mathrm{eff}},\boldsymbol{\sigma})}{\partial \boldsymbol{H}_{\mathrm{eff}}}\right)^{\mathrm{T}} \tag{12}$$

$$\boldsymbol{d} = \boldsymbol{M}_{\mathrm{an}} - \boldsymbol{M}_{\mathrm{irr}} \quad \text{and } \delta = \frac{d\boldsymbol{B}}{dt}\cdot\boldsymbol{d} \tag{13}$$

$$\frac{d\boldsymbol{M}_{\mathrm{irr}}}{d\boldsymbol{H}_{\mathrm{eff}}} = \begin{cases} \boldsymbol{k}(\boldsymbol{\sigma})^{-1}\dfrac{\boldsymbol{d}\boldsymbol{d}^{\mathrm{T}}}{\|\boldsymbol{d}\|}, & \text{if } \|\boldsymbol{d}\| > 0 \quad \text{and } \delta > 0 \\ \boldsymbol{0}, & \text{otherwise,} \end{cases} \tag{14}$$

$$\frac{d\boldsymbol{M}}{d\boldsymbol{H}_{\mathrm{eff}}} = c\frac{d\boldsymbol{M}_{\mathrm{an}}}{d\boldsymbol{H}_{\mathrm{eff}}} + (1-c)\frac{d\boldsymbol{M}_{\mathrm{irr}}}{d\boldsymbol{H}_{\mathrm{eff}}} \tag{15}$$

in which $\boldsymbol{H}_{\mathrm{eff}}$ is the effective field strength experienced by the domains, and $\boldsymbol{M}_{\mathrm{an}}$ and $\boldsymbol{M}_{\mathrm{irr}}$ are the anhysteretic and irreversible components of the total magnetization. α and c are fitting parameters. The stress-dependence is included in the model through (12), in which the anhysteretic constitutive law, derived in the previous section, is used. The tensor parameter $\boldsymbol{k}$ describes the magnitude of domain-wall pinning and is also made stress-dependent in order to describe the change of the hysteresis losses with stress. Since hydrostatic pressure is known not to affect magnetic properties [4], $\boldsymbol{k}$ becomes a function of the deviatoric part $\boldsymbol{s}$. The tensorial integrity basis for a second-order tensor in 3-D space is $\{\boldsymbol{I}, \boldsymbol{s}, \boldsymbol{s}^2\}$, and thus $\boldsymbol{k}(\boldsymbol{s})$ can be expressed as

$$\boldsymbol{k}(\boldsymbol{s}) = k_0(\boldsymbol{I} + a\boldsymbol{s} + b\boldsymbol{s}^2) \tag{16}$$

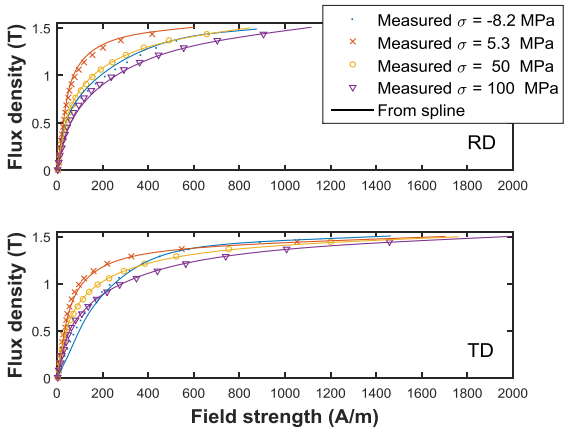

Fig. 2. Comparison of measured and modeled single-valued $B(H)$ curves of Material 1 in the RD and TD. The measured curves have been obtained by averaging the major hysteresis loop in the H-direction.

in which the parameters k_0, a, and b can depend only on the scalar invariants $\mathrm{tr}(\boldsymbol{s}^2)$ and $\det(\boldsymbol{s})$. In this paper, they are constant and treated as fitting parameters.

D. Extension for Orthotropic Anisotropy

The isotropic model can be extended to an orthotropic case by replacing the scalar coefficients $p_{mn,ij}$ in (10) with tensors

$$\boldsymbol{p}_{mn,ij} = p_{1,mn,ij}\boldsymbol{E}_1 + p_{2,mn,ij}\boldsymbol{E}_2 + p_{3,mn,ij}\boldsymbol{E}_3 \qquad (17)$$

where $\boldsymbol{E}_l = \boldsymbol{e}_l \otimes \boldsymbol{e}_l$ and $p_{l,\mathrm{mn},\mathrm{ij}}$, $l = 1, 2, 3$, respectively, are the structural tensors corresponding to the orthotropic symmetry group and the coefficients of their linear combination. Vectors $\boldsymbol{e}_l$ are mutually orthogonal unit vectors and $\otimes$ designates the tensor product. In orthotropic case, $\boldsymbol{E}_1 + \boldsymbol{E}_2 + \boldsymbol{E}_3 = \boldsymbol{I}$. We place the RD in the x-direction and TD in the y-direction, and assume all the magnetic fields to lie in the xy plane. Thus only $p_{\mathrm{x},mn,ij}$ and $p_{\mathrm{y},mn,ij}$ need to be identified.

Following the idea of [7], the JA-model parameters α, c, k_0, a, and b are also replaced by the corresponding tensors $\boldsymbol{\alpha}$, $\boldsymbol{c}$, $\boldsymbol{k}_0$, $\boldsymbol{a}$, and $\boldsymbol{b}$. The scalar 1 in (15) is replaced by $\boldsymbol{I}$. Also in this case, only the xx and yy components of the tensor parameters need to be identified from measurements.

III. Application and Results

A. Identification of the Model

The spline coefficients $p_{\mathrm{x},mn,ij}$ and $p_{\mathrm{y},mn,ij}$ are identified by integrating the bi-cubic energy-density spline separately from the unidirectional measurement data for the RD and TD. For Material 1, $B(H)$ curves measured at nine compressive ($-$) and tensile (+) stresses ranging from -8.2 to 100 MPa are considered in the identification. For Material 2, nine tensile stresses ranging from 0 to 94 MPa are considered. Single-valued curves are extracted from the measurements by averaging the hysteresis loops in the H-direction. Fig. 2 shows that the $B(H)$ curves obtained from the anhysteretic constitutive law correspond well to the measured ones for Material 1. Similar correspondence is obtained for Material 2.

TABLE I
Hysteresis Model Parameters for the Materials in RD and TD

RD	Material 1	Material 2	TD	Material 1	Material 2	Unit
c_{xx}	0.221	0.353	c_{yy}	0.284	0.300	-
α_{xx}	9.13	7.44	α_{yy}	12.4	11.1	10^{-5}
$k_{0\mathrm{xx}}$	78.0	78.6	$k_{0\mathrm{yy}}$	108	94.4	A/m
a_{xx}	-322	-181	a_{yy}	74.6	-672	$(\mathrm{GPa})^{-1}$
b_{xx}	7950	3770	b_{yy}	3290	7460	$(\mathrm{GPa})^{-2}$

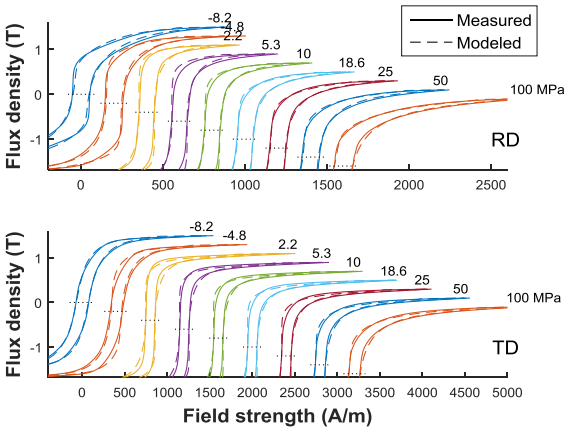

Fig. 3. Comparison of measured and modeled hysteresis loops of Material 1 in the RD and TD. The curves at stresses greater than -8.2 MPa have been shifted from the origin for clarity. The peak value of flux density is the same for all the curves. The dotted line show the $B = 0$ level for each curve.

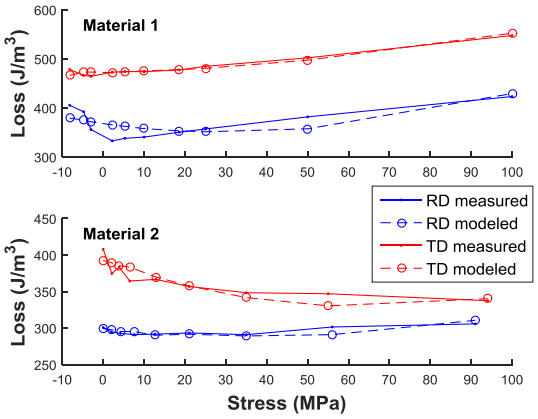

Fig. 4. Comparison of measured and modeled energy loss densities under uniaxial stress and a parallel magnetic field in the RD and TD for the two materials. The measured losses have been obtained at 3 Hz.

The JA-model parameters are fitted separately for the RD and TD using a nonlinear least-squares minimization algorithm. The obtained parameters are shown in Table I. Fig. 3 compares the modeled and measured hysteresis loops at the chosen stresses for Material 1. Largest differences are obtained close the knee points, which is rather typical for the JA model. The hysteresis losses for both materials are compared in Fig. 4. Due to the chosen quadratic dependence of $\boldsymbol{k}$ on $\boldsymbol{s}$ in (16) the model doesn't account for the very steep change in the losses around zero stress in Material 1. However, the nonmonotonous trend in the hysteresis loss versus stress is still visible. In Material 2, the losses in the RD are almost

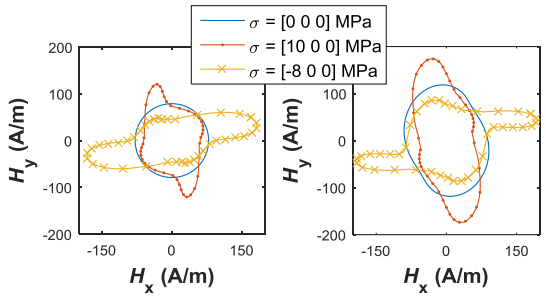

Fig. 5. Field strength loci under different in-plane stress tensors (in notation $[\sigma_{xx}\sigma_{yy}\sigma_{xy}]$) and circular flux density of 1.0 T in Material 1. (a) Isotropic case (only RD parameters used) and (b) anisotropic case.

constant, while the losses in the TD decrease monotonically under tension.

B. Behavior Under Rotational Fields

The model is numerically tested for Material 1 under rotational flux-density and uniaxial stresses in the RD. Even under tensile stress, the rotation of the field makes it necessary to utilize also the compressive measurement data in the interpolation of $\phi_{\mathrm{me},u}$ and $\phi_{\mathrm{me},v}$. For example, if the uniaxial stress in the x-direction is σ, the deviatoric stress components are $s_{xx} = 2\sigma/3$ and $s_{yy} = s_{zz} = -\sigma/3$. Thus $I_5 = H_x s_{xx} + H_y s_{yy}$ becomes negative when the angle of the magnetic field is between $\arctan(-s_{xx}/s_{yy}) = \arctan(2) \approx 63.4°$ and 90°.

We first consider an isotropic version of the model, in which only the RD parameters are used. Fig. 5(a) shows the field strength loci under a rotating flux density vector with amplitude of 1.0 T. It is seen that larger field strengths are required in the directions perpendicular to tension and parallel to compression. When the field strength in (3) points perpendicular to the uniaxial stress, I_5 equals -0.5 times the value obtained when the field is parallel to the stress. Thus the 10 MPa tension applied in the x-direction acts as a 5 MPa compression in the y-direction. Compression reduces the permeability much more drastically than tension, and thus a higher field strength is needed in the y-direction. This effect is also observed in the measurements of [8]. When the field strength points 63.4° from the uniaxial stress, I_5 becomes zero and the stress has no effect on the anhysteretic magnetization.

Fig. 5(b) shows the corresponding field-strength loci when the anisotropy is considered. It is apparent that higher field strength is required in the TD than in Fig. 5(a). Similar to the results in [8, Fig. 7(e)], the field strength decreases parallel to tension and perpendicular to compression, and increases vice versa. However, measurements under rotational fields and multiaxial stress on the studied material would be needed to accurately check the validity of the curves.

It is noteworthy that the consideration of hysteresis causes the loci not to be symmetric with respect to the RD and TD axes. When the angle of $\boldsymbol{H}$ with respect to the unidirectional stress is 45°, the angle of $\boldsymbol{M}$ with respect to the stress is $< 45°$, since it lags the field strength. However, when the angle of $\boldsymbol{H}$ is 135°, meaning again 45° from the unidirectional stress, the angle of $\boldsymbol{M}$ with respect to the stress is $>45°$.

IV. Discussion and Conclusion

A magnetic material model accounting for anisotropy and stress-dependent hysteresis was proposed and fitted for two different materials. The model combines a reversible thermodynamic constitutive law to the vector JA model for hysteresis. Extrapolation of the cubic spline free energy expression to field strengths (or values of u) higher than the measured ones can be done, for example, by fitting analytical models for the single-valued $B(H)$ curves at constant stresses. However, extrapolation to higher stresses (or values of v) is very difficult, since such analytical models are not available. The model is thus guaranteed to work only in the range of measured v values.

Under rotational flux density excitation, the field strength loci predicted by the model are very sensitive to the smoothness of the interpolation of the energy density with respect to variable v in (6). As discussed above, a rotating field and uniaxial stress σ cause v to obtain values in the range from $-\sigma/3$ to $2\sigma/3$. In order to obtain smooth and physically reasonable field strength loci, the measured data should be as smooth as possible over the whole stress range.

Acknowledgment

The research leading to these results has received funding from the European Research Council under the European Union's Seventh Framework Programme (FP7/2007-2013) / ERC grant agreement n°339380. The work of P. Rasilo was supported by the Academy of Finland. The work of S. Steentjes was supported in part by the DFG by the research group "FOR 1897–Low-Loss Electrical Steel for Energy-Efficient Electrical Drives" and in part by the project "Improved Modeling and Characterization of Ferromagnetic Materials and Their Losses."

References

[1] N. Leuning, S. Steentjes, M. Schulte, W. Bleck, and K. Hameyer, "Effect of elastic and plastic tensile mechanical loading on the magnetic properties of NGO electrical steel," *J. Magn. Magn. Mater.*, vol. 417, pp. 42–48, Nov. 2016.

[2] L. Daniel, M. Rekik, and O. Hubert, "A multiscale model for magneto-elastic behaviour including hysteresis effects," *Arch. Appl. Mech.*, vol. 84, no. 9, pp. 1307–1323, 2014.

[3] K. Yamazaki and Y. Kato, "Iron loss analysis of interior permanent magnet synchronous motors by considering mechanical stress and deformation of stators and rotors," *IEEE Trans. Magn.*, vol. 50, no. 2, pp. 909–912, Feb. 2014.

[4] L. Daniel, "An analytical model for the effect of multiaxial stress on the magnetic susceptibility of ferromagnetic materials," *IEEE Trans. Magn.*, vol. 49, no. 5, pp. 2037–2040, May 2013.

[5] L. Daniel, O. Hubert, and M. Rekik, "A simplified 3-D constitutive law for magnetomechanical behavior," *IEEE Trans. Magn.*, vol. 51, no. 3, Mar. 2015, Art. no. 7300704.

[6] P. Rasilo *et al.*, "Modeling of hysteresis losses in ferromagnetic laminations under mechanical stress," *IEEE Trans. Magn.*, vol. 52, no. 3, Mar. 2016, Art. no. 7300204.

[7] J. Gyselinck, P. Dular, N. Sadowski, J. Leite, and J. P. A. Bastos, "Incorporation of a Jiles-Atherton vector hysteresis model in 2D FE magnetic field computations: Application of the Newton–Raphson method," *COMPEL-Int. J. Comput. Math. Elect. Electron. Eng.*, vol. 23, no. 3, pp. 685–693, 2004.

[8] Y. Kai, Y. Tsuchida, T. Todaka, and M. Enokizono, "Influence of stress on vector magnetic property under rotating magnetic flux conditions," *IEEE Trans. Magn.*, vol. 48, no. 4, pp. 1421–1424, Apr. 2012.